Susceptibility Weighted Imaging (SWI)

E. Mark Haacke,[1-4]* Yingbiao Xu,[1,2] Yu-Chung N. Cheng,[1] and Jürgen R. Reichenbach[5]

Susceptibility differences between tissues can be utilized as a new type of contrast in MRI that is different from spin density, T_1-, or T_2-weighted imaging. Signals from substances with different magnetic susceptibilities compared to their neighboring tissue will become out of phase with these tissues at sufficiently long echo times (TEs). Thus, phase imaging offers a means of enhancing contrast in MRI. Specifically, the phase images themselves can provide excellent contrast between gray matter (GM) and white matter (WM), iron-laden tissues, venous blood vessels, and other tissues with susceptibilities that are different from the background tissue. Also, for the first time, projection phase images are shown to demonstrate tissue (vessel) continuity. In this work, the best approach for combining magnitude and phase images is discussed. The phase images are high-pass-filtered and then transformed to a special phase mask that varies in amplitude between zero and unity. This mask is multiplied a few times into the original magnitude image to create enhanced contrast between tissues with different susceptibilities. For this reason, this method is referred to as susceptibility-weighted imaging (SWI). Mathematical arguments are presented to determine the number of phase mask multiplications that should take place. Examples are given for enhancing GM/WM contrast and water/fat contrast, identifying brain iron, and visualizing veins in the brain. Magn Reson Med 52:612–618, 2004. © 2004 Wiley-Liss, Inc.

Key words: magnetic susceptibility; phase imaging; water/fat separation; artery/vein separation; imaging iron

A number of important tissues have unique magnetic susceptibility differences relative to background or surrounding tissues. One such example is partially deoxygenated venous blood (1–3). Other examples include clot (paramagnetic), calcium (diamagnetic) (4), and iron-laden tissue (5), and air/tissue interfaces. These bulk magnetic susceptibilities are indistinguishable from chemical shift effects. The most common example of the latter in magnetic resonance imaging (MRI) is the chemical shift difference between water and fat. Usually chemical shift effects are ignored, but in the case of water and fat separation (6–8) the 3.35-ppm difference is used to separate water and fat. On the other hand, if information regarding several species occupying the same voxel is desired, one usually obtains the spectral information by collecting a time series of data and Fourier transforming the data. This is referred to as chemical shift imaging.

However, when only a single element or tissue component is present in a voxel, or if there is a dominant element in each voxel, it is possible in some circumstances to extract spectral information from the phase alone. The phase image itself can then be used to separate the dominant spectral information on a pixel-by-pixel basis. This concept has been used in a single point water/fat separation approach (7) and in imaging velocity using phase in MR angiography (MRA) (9). The problem with phase images has generally been the presence of background local fields that confound the effects of local phase changes in tissue. However, when the phase changes between tissues have a high spatial frequency, these unwanted global effects essentially can be removed (8). Once this is accomplished, the door is open for new applications of phase imaging to highlight or differentiate one type of tissue from another. First, the phase itself can be a superb source of image contrast. This has already been demonstrated for GM/WM contrast (10), small veins in the brain (11), and more recently in venous blood vessels in the peripheral vasculature (8). Second, the phase can be used as a mask to create magnitude images with suppressed/enhanced spectral components or modified contrast. Third, the phase images themselves can be used to create projection images to show tissue (vessel) contiguity. Here we consider single time point methods to enhance the contrast of certain tissues containing fat, venous blood, or iron. Since we focus on the role of susceptibility, and use the original phase image both by itself and as a means of altering the contrast in the magnitude images, we refer to this method as susceptibility weighted imaging (SWI) (12).

Although SWI has been used as an MR venographic method for several years (13–26), it has more recently been applied to studies of arterial venous malformations (16,24), occult venous disease (15), multiple sclerosis (20), trauma (25), tumors (21,23,26), and functional brain imaging (14,22). Given the continued increasing clinical interest in this topic, it is important to ensure a complete understanding of the mathematical processes involved in creating SW images.

MATERIALS AND METHODS

Our goal in this work was to use phase to enhance contrast between tissues with different susceptibilities. This can be accomplished in several steps. First, we employ the high-pass filter described in Ref. 8 to remove the low-spatial-frequency components of the background field. In the work shown here, we use a 64×64 low-pass filter and divide this into the original phase image (512×512) to create a high-pass filter effect.

Second, this "corrected" phase image is used to create a "phase" mask that is used to multiply the original magni-

tude image to create novel contrasts in the magnitude image. The phase mask is designed to suppress those pixels that have certain phases. It is usually applied in the following manner: If the minimum phase of interest is, for example, $-\pi$, then the phase mask is designed to be $f(x) = (\varphi(x) + \pi)/\pi$ for phases < 0, and to be unity otherwise, where $\varphi(x)$ is the phase at location x. That is, those pixels with a phase of $-\pi$ will be completely suppressed and those with a value between $-\pi$ and zero phase will be only partly suppressed. This phase mask (f(x)) then takes on values that lie between zero and unity. We will refer to it as the negative phase mask. It can be applied any number of times (integer m) to the original magnitude image ($\rho(x)$) to create a new image $f^m(x)\rho(x)$ with different contrasts (11,13,22). Another mask might be defined to highlight positive phase differences:

$$\rho(x)_{new} = g^m(x)\rho(x) \qquad [1]$$

If the maximum phase of interest is, for example, π, then the phase mask is designed to be $g(x) = (\pi - \varphi(x))/\pi$ for phase > 0, and unity otherwise. We will refer to this as the positive phase mask.

Alternatively, if echo times (TEs) are so long that they cause difficulties, or if it is desirous to calculate phase from very short TEs without any RF penetration phase effects, an interleaved double-echo scan can (29) be acquired to simulate the equivalent phase of a short-TE scan. The complex data from the first echo are then divided into those of the second echo to create an equivalent phase image to that for a TE of ΔTE. That is, the phase in the complex division becomes $-\gamma\Delta B\Delta TE$. We use this concept to create an effective TE = 2 ms image from an interleaved TE = 8 ms and TE = 10 ms data set.

All sequences used in this study were high-resolution, 3D gradient-echo scans. In-plane resolution varied from 0.5 mm $\times$ 0.5 mm to 1 mm $\times$ 1 mm with slice thicknesses of 0.7–2 mm. Except for the interleaved double-echo experiment for highlighting fat described above, the experiments were run with TE = 40 ms. These experiments were all performed at 1.5T except for one case in which the data were obtained at 3.0T.

Phase Mask Multiplication: Theoretical Considerations

Phase masks are created to enhance the contrast in the original magnitude images. Depending on the constructs used to create the filter, the number of multiplications needed to optimize the contrast-to-noise ratio (CNR) in the SW images will vary. We consider the positive phase mask case below. The results for the negative phase mask follow by letting φ go to $-\varphi$. The first step is to write an expression for the CNR between two tissue types. Consider first the example in which all tissues have the same signal S_0 with Gaussian noise, and contrast is generated only by the phase images. The contrast in the magnitude image is therefore zero. Contrast appears only after multiplication by the phase mask has been performed. We create a function that is dependent on m, the number of multiplications that are performed with the phase mask. The goal is to optimize m or, equivalently, find the point at which CNR(m) is maximized. The region of the object where there is a phase difference will then change its signal after

multiplication with the phase mask. For the positive phase mask considered here, the multiplication factor of the signal will become $(1-\varphi/\pi)^m$ in the positive-phase region, while that in the negative-phase region remains unity. The inherent contrast that develops will then be $1-(1-\varphi/\pi)^m$ times S_0 of the object in the original magnitude image. The noise in the new image must take into account the noise in the original image plus the noise generated from the multiplications. For a high signal-to-noise ratio (SNR) in the magnitude images ($>4:1$), the variance of the final image after m multiplications is given by

$$\sigma_t^2 = \sigma_o^2(1 + (m/(2\pi))^2 + (1-\varphi/\pi)^{2m} + (m/\pi)^2(1-\varphi/\pi)^{2m-2} \qquad [2]$$

where σ_o is the standard deviation (SD) of the Gaussian noise in the original magnitude image (see the Appendix for a full derivation). Therefore, the functional form for CNR(m) is the contrast divided by the noise, and is given by

$$CNR(m) = SNR_0(1 - (1-\varphi/\pi)^m)/sqrt(1 + (m/(2\pi))^2 + (1-\varphi/\pi)^{2m} + (m/\pi)^2(1-\varphi/\pi)^{2m-2} \qquad [3]$$

where SNR_0 is the original SNR (i.e., S_0/σ_o). When the exponential decay of the MR signal is included in our analysis, the CNR(m) becomes:

$$SNR_0 exp(-\varphi/\pi)(1 - (1-\varphi/\pi)^m)/sqrt(1 + (m/(2\pi))^2 + (1-\varphi/\pi)^{2m} + (m/\pi)^2(1-\varphi/\pi)^{2m-2} \qquad [4]$$

where we have assumed that TE/T_2^* is unity when $\varphi = \pi$ (since it is just the increase in signal for shorter TE and hence smaller m that we are after here). The more general form can be obtained by replacing $exp(-\varphi/\pi)$ with $exp((-\varphi/\pi)T_2^*/TE)$.

However, T_2^* plays a role in the signal decay, and we can not arbitrarily choose a long TE to get the phase to be π without a great loss in SNR. Thus, when the phase is π, there will be circumstances in which the number of multiplications required will be >1 in order to show the optimal contrast in the images. This raises an interesting question. If one is willing to spend a fixed amount of time imaging (specifically, to acquire a long enough TE to ensure that the phase is π), then it is not clear whether a shorter TE with more phase multiplications might not do just as good a job. That is, it might be better to look into reducing the TE (and hence the TR), collecting the data with a shorter TE (i.e., with a higher signal), performing more multiplications, and averaging over several acquisitions in order to obtain an optimal CNR.

For the case of the same volume coverage as well as the same imaging time, one then considers the efficiency CNR*sqrt(number of slices)/sqrt(time) rather than the CNR. This introduces another factor of sqrt(π/φ) into the right-hand side of Eq. [4] such that CNR is proportional to (although we ignore the need to increase the read gradient strength when TR becomes too short):
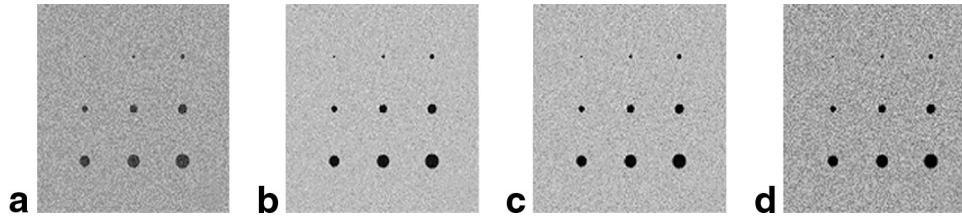
FIG. 1. Simulated images with the phase mask multiplied (**a**) once, (**b**) four times, (**c**) eight times, and (**d**) 16 times. The radius of the circles varied from one to 16 pixels. All circles have the same phase value of 0.3 π. The SNR of the original magnitude image was 15:1.

$$SNR_0 sqrt(\pi/\varphi)exp(-\varphi/\pi)(1 - (1-\varphi/\pi)^m)$$
$$/sqrt(1 + (m/(2\pi))^2$$
$$+ (1-\varphi/\pi)^{2m} + (m/\pi)^2(1-\varphi/\pi)^{2m-2}) \quad [5]$$

This term arises because the only way to collect these data is to either increase the overall time by acquiring the data a second time or use a segmented echo-planar-like approach, which in turn requires that the gradient strength be increased accordingly. When the gradient strength is increased (such that both the sampling time and TE are decreased), then a factor of $sqrt(\varphi)$ loss in SNR occurs, and Eq. [5] reduces once again to Eq. [4].

If one is interested in comparing images with circular objects of radius p pixels, (Fig. 1) then one can look at visibility $\mathcal{V}$ instead of CNR (29), where

$$\mathcal{V} = CNR(m)*p \, sqrt(\pi) \quad [6]$$

In the plots for Figs. 2 and 3, we have taken p = 2.

Phase Mask Multiplication: Simulations

We created a series of circles by simulating a Fourier transform experiment with a 512 × 512 acquisition matrix (i.e., pixels). The radius of the circles varies from one to 16 pixels (see Fig. 1). Within each circle, the phase value is set to be 0.3π. The initial signal intensity of all pixels within the image is set to be 1500. A Gaussian noise with an SD of 100 is added to each real and imaginary channel. Finally, a magnitude image and a phase image are reconstructed from the real and imaginary channels. The SNR of the magnitude image is then 15:1. A region of interest (ROI) is drawn inside and outside of each circle to obtain the CNR between the two ROIs.

RESULTS

Number of Multiplications

The predictions of Eq. [3] are shown in Fig. 2a. They validate previous work in this area (11,13), and indicate that three to five multiplications provide the best contrast when the veins are enhanced. The veins vary in their phase behavior, with those perpendicular to the main field having a phase of at most $-\pi/2$. In that case, CNR(m) is predicted to peak for m = 4. However, many vessels will be partial-volumed (even those parallel to the main field) so that there will be a spread of phases. The lower the phase, the larger the m necessary to obtain the optimal contrast; however, an m of 3–5 is shown to create good

contrast for many different values of φ. To test the theory more extensively, we compare next the measured values of CNR(m) for the simulated data described above. We plot the results in Fig. 2b. The results are in good agreement, given the approximations made about large SNR. The simulated images in Fig. 1 demonstrate that the best CNR is obtained with an m of about 4, but even an m of 8 gives a good CNR. The image with an m of 16 is clearly as noisy as the image with m equal to one. From a practical point of view, given that noise is increased as m increases, the best value of m to choose is the smallest one that meets the desired CNR. This is particularly true if a minimum intensity projection (mIP) is to be performed afterward, because the more noise that is present, the worse the mIP will be. As discussed above, there will be times when it may be more expedient to collect the data at shorter TE but in a given fixed total time period. The results of these predictions are shown in Fig. 3. The curves suggest that choosing a TE such that the phase is 0.3 π (Eq. [5]) to 0.5 π (Eq. [4]) may be the best way to collect the data for optimal SNR and spatial coverage.
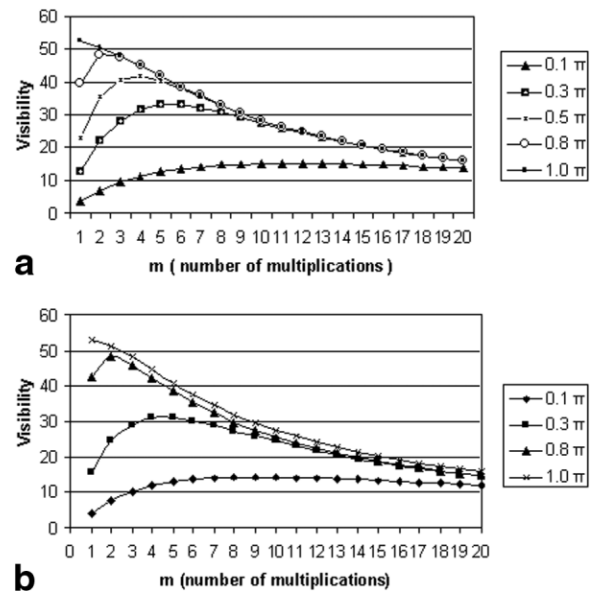

FIG. 2. **a:** Visibility as a function of multiplication (2sqrt(π) × Eq. [3]). Note that the smaller the phase value, the larger the multiplication required to reach the maximum CNR. **b:** Visibility as measured in the simulated images in Fig. 1 as a function of multiplication. Note that the results are in good agreement with the theoretical predictions shown in a.
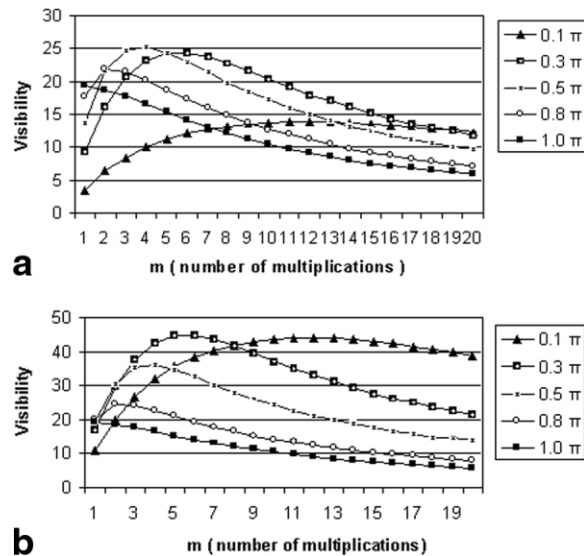
FIG. 3. Plots of visibility show the predictions of (**a**) $\mathcal{V}$/sqrt(time) and (**b**) $\mathcal{V}$/sqrt(number of slices)/sqrt(time) as a function of the number of multiplication (2sqrt(π) $\times$ Eq. [4] and 2sqrt(π) $\times$ Eq. [5]). The curves suggest that choosing a TE such that the phase is (**a**) 0.5 π or (**b**) 0.3 π may be the best way to collect the data for optimal SNR and optimal coverage, respectively.

Filtered Phase Imaging

This example focuses on visualizing water and fat in a single image. Here we use the data acquired from a double gradient-echo scan with TEs of 8 and 10 ms. The magnitude image from the TE = 8 ms image is shown in Fig. 4a. By complex-dividing the TE = 8 ms image into the TE = 10 ms image, we create a phase image with ΔTE = 2 ms (Fig. 4b). Such a short TE avoids the problems associated with aliasing caused by the inhomogeneities near the air/tissue interfaces in the sinuses near the orbit for the original longer-TE scans. This value of 2 ms was chosen to obtain fat roughly π out of phase with water (although this condition is not necessary in order for the method to work). The resulting phase images are essentially alias-free and well smoothed compared to the original data. The phase itself clearly discriminates water and fat without the need for any anti-aliasing programs or fat saturation. The optic nerve is well shown, buried in the surrounding muscle.

Enhancing Magnitude Contrast

Continuing with the water/fat example, when the negative phase mask is used once, the fat is nicely suppressed (Fig. 4c); however, when it is used twice, the fat is dramatically reduced in amplitude but is not eliminated (Fig. 4d). The former image gives excellent contrast in the T_1-weighted image, which still includes some fat signal (this is still of value when the images are clinically reviewed). A separate fat image can be obtained by subtracting this image from the original unprocessed image, or by just using the phase image itself as a means of visualizing the water and fat separately.

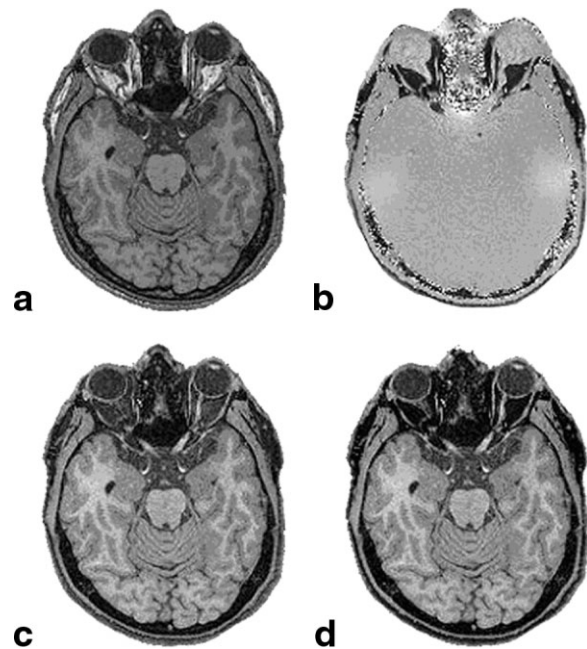A second application of the phase images is the enhancement of GM/WM contrast in T_1-weighted imaging.

FIG. 4. A demonstration of the visualization of fat and water with phase information. **a:** The original magnitude image with TE = 8 ms. **b:** The equivalent TE of the 2 ms phase image resulting from the complex division of TE = 10 ms and 8 ms images. **c** and **d:** SW images of part **a** after the phase mask (**b**) was multiplied one and two times, respectively. Note that the fat signal is effectively suppressed around the optic nerve in **c** and **d**.

We ran a T_1-weighted scan with TE = 5 ms, and then followed this with an SWI scan with TE = 40 ms on a 1.5T system. Both scans have the same resolution (0.5 mm $\times$ 1 mm $\times$ 2 mm) and cover the same ROI. Figure 5a shows the 5-ms data. We used the phase image of the same slice position from the 40-ms data set of the SW scan to create a phase mask. Then we multiplied the phase mask into the magnitude image (Fig. 5a) four times to create a phase-masked image (Fig. 5b), which showed an enhanced con-
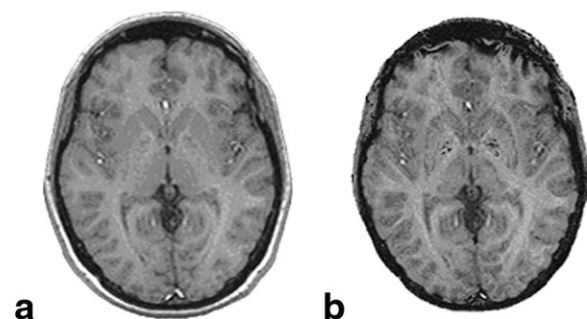

FIG. 5. A demonstration of the utilization of the phase image from SWI to enhance GM/WM contrast in T_1-weighted imaging. **a:** T_1-weighted magnitude image of TE = 5 ms. **b:** The same magnitude image as in part **a**, with m = 4 using the phase mask from the TE = 40 ms data. Note the enhanced contrast between GM and WM in the lower half of the image. Some mineralization in the globus pallidus is also revealed. Some artifacts are introduced at the top of the image because of the local field inhomogeneity caused by the sinus.
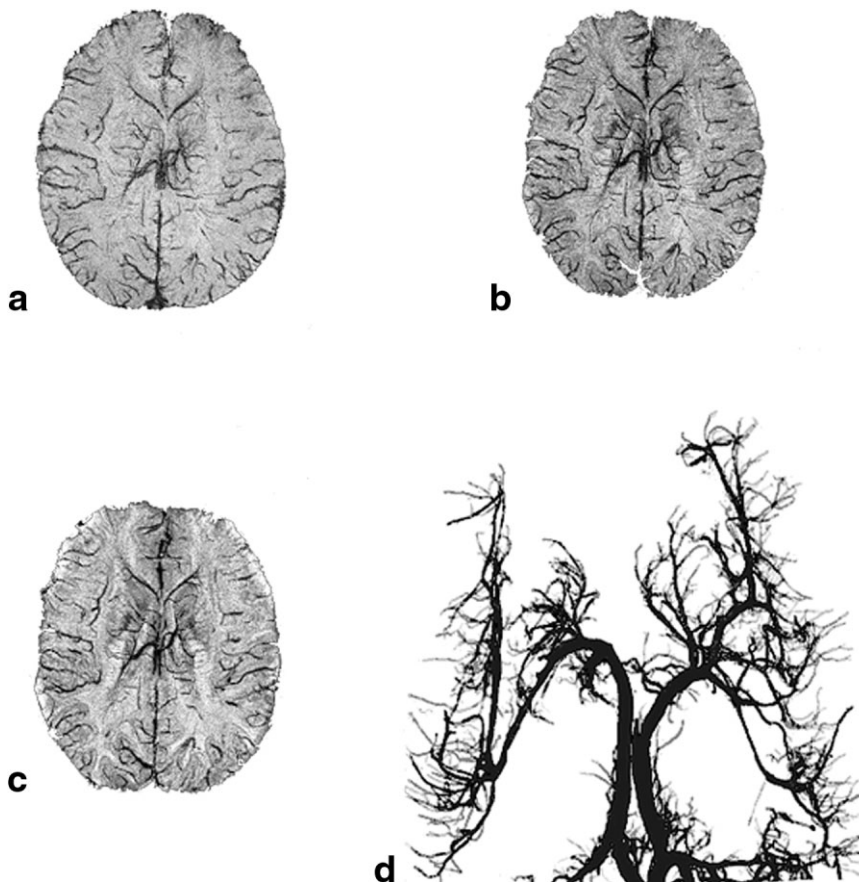
FIG. 6. **a:** mIP of the original magnitude images without any phase mask multiplication. **b:** Modified mIP of SW images using m = 4. **c:** mIP of filtered phase images. **d:** A slice from a cadaver brain, which can be compared to the middle section of the images shown in **a–c.** (Image courtesy of Dr. Georges Salamon.) Note that the increased contrast enhancement in **b** compared to **a** originates from the phase contrast shown in **c.** These images were collected at 3.0T.

trast and better edge definition as well (although, as expected, the image was a little noisier).

As a third example of phase-enhanced magnitude contrast, we revisit the application to the venous blood vessels in the brain. Given that the susceptibility difference between fully oxygenated and deoxygenated blood is 0.18 ppm in cgs units, as reported in Ref. 28, a rather long TE of 40 ms is required to visualize large phase differences. Vessels parallel to the field will show a negative phase inside the vessels, and those perpendicular to the field will show a positive phase inside the vessels (29). However, due to finite voxel size (and hence partial volume effects), as well as aliasing of the external fields outside the vessels, the perpendicular vessels may appear to have a negative phase when the resolution is low. In Fig. 6, we show an example from a 3T system with a resolution of 0.5 mm × 0.5mm × 1.0 mm. The data set was collected in a transverse orientation, with the z-direction (the main field direction) being slice-select (i.e., the slices are 1 mm thick). To demonstrate the value of the phase mask, we show in Fig. 6a and 6b an mIP over 12 slices without and with, respectively, the special phase processing. Actually, the phase images themselves can be mIPped (Fig. 6c), and they reveal why this method works so well: all of the vessels that are enhanced over and above the cancellation already present in the magnitude images are shown in this mIP. This is the first time that phase images have been used to generate a projection that in and of itself has potential value.

DISCUSSION AND CONCLUSIONS

Phase images contain direct information about the background magnetic field and chemical shift of tissues. The ability to use the phase for spectroscopic information depends, in part, on the elimination of phase from the background field, and partial volume effects with other tissues that have different chemical shifts. When it comes to the ideal choice of mask multiplication, partial volume effects can modify the simple arguments of a one-compartment model. In these cases, a series of multiplications may be best—or at least that image that can simultaneously enhance the contrast for all cases would be the best image to display. For example, if the blood vessel is so small that a phase of 90° turns into a phase of 45°, then it will take more multiplications to bring out a better contrast. Those vessels that still show phases of 90° will not be hurt much by the use of more multiplications. This special number of multiplications usually turns out to be about 3, 4, or 5. This choice also keeps the CNR drop to a factor of less than sqrt (2). From Fig. 2, we can see there is a trade-off between the gain of CNR and loss of SNR by means of phase multiplication before CNR reaches its peak. Afterwards, CNR and SNR both decrease as the number of multiplications increases.

Number of Multiplications

Although partial volume effects are often problematic, they turn out to be rather useful in our implementation of

the phase-masking process. For vessels perpendicular to the main field, we expect the phase to be positive inside the vessel when the vessel is the size of a pixel. The partial volume effect apparently reverses this behavior for transverse images when the vessel is smaller than the in-plane voxel size, and the slice is twice as thick (or more) as the in-plane voxel size. The phase now appears to be negative but much smaller than π. As shown in Fig. 3, even with a lower phase value, we can enhance the presence of a vessel by performing a phase mask with m about 4. This is demonstrated in Fig. 6c, where the phase of the perpendicular vessels is clearly negative and varies from vessel to vessel.

At longer TE, if the phase at the boundary aliases, the phase multiplication results in fatter vessels. There is a potential problem here. In more complicated cases, the phase might change sign and make the processing less effective and the interpretation of the resulting images less clear. However, in practice this has not been a problem. One way to avoid this difficulty is to use constant time imaging, which allows for a reduced TE but does not require a large phase shift. To overcome this, more multiplications must be performed (up to eight to 10 for a phase of only 0.1 π; Fig. 3b). Nevertheless, it is quite interesting that such a low phase difference can lead to an excellent increase in contrast. This may have important implications for observing areas of small changes in iron content or small blood vessels.

Water/Fat Separation

In Fig. 4, the effective TE time is 2 ms. This value was chosen so that we could obtain fat roughly π radians out of phase with water (although this is not a necessary condition for this method to work), so that with one or two multiplications the fat signal would be effectively suppressed. With this effective short TE, we can see the strong differences between the complicated phase in the original images and the unwrapped phase image (Fig. 4b). With high resolution to reduce the partial volume effect, and high bandwidth to reduce the signal shift from fat, this means of suppressing fat becomes more viable. Nowadays, the TE can be < 2 ms for a fast gradient-echo sequence, so without having to acquire a data set twice to create the equivalent short-TE phase image (as in Fig. 4), we can use the phase image itself by filtering out the background phase effects first to do the same job. The phase image clearly discriminates between water and fat without the need for any anti-aliasing programs or fat saturation when small TEs are used. The phase from global background field inhomogeneities might still add to the phase contributed by the fat chemical shift, causing aliasing. This would prevent the method from working perfectly, but for these short TEs this is unlikely to be a problem.

Phase Filtering

At these long TEs, because of the excess aliasing, the high-pass filter cannot remove all the background phase effects from air/tissue interfaces, which then generate a false contrast that is not caused by vessels. However, since we know where these problems occur (such as near the sinuses), we can avoid interpreting the data in these areas.

We have tried using a multiecho approach to remove all background field effects except those due to partial voluming (i.e., small vessels only), with some success. More recent attempts have involved an alternative to homodyne filtering that works directly on the reconstructed phase images, as in Ref. 30. Further work in this area would be useful to remove remnant air/tissue field inhomogeneity effects. Finally, if these remnant errors can be removed, phase images and projections over phase images may play a more important role in presenting new contrast features.

Acquisition Time

Given the fact that this is a 3D, long-TR acquisition scheme, it can take 8 min to acquire the data with 32 partitions and a matrix size of 256 (phase) $\times$ 512 (read). Apart from the above-mentioned background field effects on the phase, this is perhaps the major impediment to this method. However, segmented EPI has the potential to reduce the imaging time by at least a factor of 2 and perhaps 4 (work in progress), and parallel imaging may reduce it by another factor of 2. Therefore, at 1.5T it will become possible to collect the data with 64 partitions in 2–4 min, while at 3T the TR can be cut in half (since the TE can be cut in half), making it possible to collect 128 slices (whole brain coverage) in just 2–4 min.

CONCLUSIONS

SWI continues to find applications in both research and clinical areas. A proper understanding of its processes is of paramount importance for obtaining images with the best contrast possible. In this work we have explained how the current processing methods work, and introduced several new concepts to enhance contrast based on the use of phase images and constant time imaging.

ACKNOWLEDGMENTS

APPENDIX

Calculation of the CNR Between two Pixels in an SW Image

In this Appendix, the CNR between two pixels in an SW image is calculated. These two pixels are labeled as one and two. In an original magnitude image, the two pixels have signals S_1 and S_2. The corresponding noises (SDs of the Gaussian noises) in the two pixels are σ_1 and σ_2 such that the SNRs are SNR_1 ($= S_1/\sigma_1$) and SNR_2 ($= S_2/\sigma_2$), respectively. The phases of these two pixels are φ_1 and φ_2. The SDs of the corresponding pixels in the phase image are

assumed to be $d\varphi_1$ ($\approx\sigma_1/S_1$) and $d\varphi_2$ ($\approx\sigma_2/S_2$), respectively. When SNR is close to unity, the noise distribution is no longer Gaussian. In that case, the Rayleigh distribution has to be considered such that the SD of the noise can be correctly calculated.

Suppose we consider a function, $h(\varphi,m)$, that consists of m multiplications of the positive phase mask, i.e., the value of this function is $(1-\varphi/\pi)^m$ when φ is between 0 and π, and the value is set to be one when φ is between $-\pi$ and 0. When φ is positive, the SD of this function is

$$\sigma_h = (m/\pi)(1-\varphi/\pi)^{m-1}d\varphi \qquad [A1]$$

When φ is negative, the SD is zero (i.e., no noise is introduced in this region). When φ is 0, the SD is $(m/(2\pi))\,d\varphi$, where the extra factor ½ is due to the discontinuity. These results can be derived from the concept of error propagation. The SW image is created by the multiplication of the magnitude image and the function $h(\varphi,m)$. If the signal of a pixel in the magnitude image is S with noise (SD) σ, then the overall signal in the SW image is $h(\varphi,m)S$, and the noise is the square root of the variance, which is $h^2(\varphi,m)\sigma^2 + S^2\sigma_h^2$, where σ_h is the SD of $h(\varphi,m)$.

Thus, the CNR between two pixels is the difference of the SNRs of the two pixels, which is $|S_1h_1 - S_2h_2|/\sigma_t$, where σ_t is the square root of

$$h_1^2\sigma_1^2 + h_2^2\sigma_2^2 + S_1^2(\sigma_{h1})^2 + S_2^2(\sigma_{h2})^2. \qquad [A2]$$

In our simulated images, the signals in the magnitude images are uniform, i.e., $S \equiv S_1 = S_2$. The SDs of noise levels of all pixels in the magnitude images are also identical, i.e., $\sigma \equiv \sigma_1 = \sigma_2$. The phase outside the black disks is zero, i.e., $h_1(0,m) = 1$ and $S_1(\sigma_{h1}) = (m/(2\pi))\,\sigma$. Thus, the CNR between two sets of pixels is

$$CNR = SNR(1 - (1-\varphi/\pi)^m)/\sqrt{1 + (m/(2\pi))^2}$$
$$+ (1-\varphi/\pi)^{2m} + (m/\pi)^2(1-\varphi/\pi)^{2m-2}), \quad [A3]$$

where $SNR \equiv S/\sigma$. This analysis applies to the negative phase mask when φ is replaced by $-\varphi$.

REFERENCES

1. Ogawa S, Lee TM, Kay AR, Tank DW. Brain magnetic resonance imaging with contrast dependent on blood oxygenation. Proc Natl Acad Sci USA 1990;87:9868–9872.
2. Ogawa S, Lee TM. Magnetic resonance imaging of blood vessels at high fields: in vivo and in vitro measurements and image simulation. Magn Reson Med 1990;16:9–18.
3. Ogawa S, Lee TM, Nayak AS, Glynn P. Oxygenation-sensitive contrast in magnetic resonance image of rodent brain at high magnetic fields. Magn Reson Med 1990;14:68–78.
4. Yamada N, Imakita S, Sakuma T, Takamiya M. Intracranial calcification on gradient-echo phase image: depiction of diamagnetic susceptibility. Radiology 1996;198:171–178.
5. Ogg RJ, Langston JW, Haacke EM, Steen RG, Taylor JS. The correlation between phase shifts in gradient-echo MR images and regional brain iron concentration. Magn Reson Imaging 1999;17:1141–1148.
6. Dixon WT. Simple proton spectroscopic imaging. Radiology 1984;153:189–194.
7. Haacke, EM, Patrick JL, Lenz GW, Parrish T. The separation of water and lipid components in the presence of field inhomogeneities. Rev Magn Reson Med 1986;1:123–154.
8. Wang Y, Yu Y, Li D, Bae KT, Brown JJ, Lin W, Haacke EM. Artery and vein separation using susceptibility-dependent phase in contrast-enhanced MRA. J Magn Reson Imaging 2000;12:661–670.
9. Bryant DJ, Payne JA, Firmin DN, Longmore DB. Measurement of flow with NMR imaging using a gradient pulse and phase difference technique. J Comput Assist Tomogr 1984;8:588–593.
10. Haacke EM, Lai S, Yablonskiy DA, Lin W. In vivo validation of the BOLD mechanism: a review of signal changes in gradient echo functional MRI in the presence of flow. Int J Imaging Syst Technol 1995;6:153–163.
11. Reichenbach JR, Venkatesan R, Schillinger DJ, Kido DK, Haacke EM. Small vessels in the human brain: MR venography with deoxyhemoglobin as an intrinsic contrast agent. Radiology 1997;204:272–277.
12. U.S. patent no. 6501272 B1, issued 31 December 2002; and U.S. patent no. 6658280, issued 2 December 2003.
13. Reichenbach JR, Essig M, Haacke EM, Lee BC, Przetak C, Kaiser WA, Schad LR. High resolution venography of the brain using magnetic resonance imaging. MAGMA 1998;6:62–69.
14. Baudendistel KT, Reichenbach JR, Metzner R, Schröder J, Schad LR. Comparison of functional venography and EPI-BOLD-fMRI at 1.5T. Magn Reson Imaging 1998;16:989–991.
15. Lee BCP, Vo KD, Kido DK, Mukherjee P, Reichenbach J, Lin W, Yoon MS, Haacke EM. MR high-resolution blood oxygenation level-dependent venography of occult (low-flow) vascular lesions. AJNR Am J Neuroradiol 1999;20:1239–1242.
16. Essig M, Reichenbach JR, Schad LR, Schönberg SO, Debus J, Kaiser WA. High-resolution MR venography of cerebral arteriovenous malformations. Magn Reson Imaging 1999;17:1417–1425.
17. Lai S, Glover GH, Haacke EM. Spatial selectivity of BOLD contrast: effects in and around draining veins. In: Moonen CRW, Bandettini PA, editors. Medical radiology. Diagnostic imaging and radiation oncology. Berlin: Springer-Verlag; 1999.
18. Lin W, Mukherjee P, An H, Yu Y, Wang Y, Vo K, Lee B, Kido D, Haacke EM. Improving high-resolution MR BOLD venographic imaging using a T_1 reducing contrast agent. J Magn Reson Imaging 1999;10:118–123.
19. Reichenbach JR, Barth M, Haacke EM, Klarhöfer M, Kaiser WA, Moser E. High-resolution MR venography at 3 Tesla. J Comput Assist Tomogr 2000;24:949–957.
20. Tan IL, van Schijndel RA, Pouwels PJW, van Walderveen MAA, Reichenbach JR, Manoliu RA, Barkhof F. MR venography of multiple sclerosis. AJNR Am J Neuroradiol 2000;21:1039–1042.
21. Reichenbach JR, Jonetz-Mentzel L, Fitzek C, Haacke EM, Kido DK, Lee BCP, Kaiser WA. High-resolution blood oxygen-level dependent MR venography (HRBV): a new technique. Neuroradiology 2001;43:364–369.
22. Reichenbach JR, Haacke EM. High-resolution BOLD venographic imaging: a window into brain function. NMR Biomed 2001;14:453–467.
23. Schad L. Improved target volume characterization in stereotactic treatment planning of brain lesions by using high-resolution BOLD MR-venography. NMR Biomed 2001;14:478–483.
24. Essig MM, Reichenbach JR, Schad LL, Debus JJ, Kaiser WA. High resolution MR-venography of cerebral arteriovenous malformations. Radiologe 2001;41:288–295.
25. Tong KA, Ashwal S, Holshouser BA, Shutter L, Herigault G, Haacke EM, Kido DK. Improved detection of hemorrhagic shearing lesions in children with post-traumatic diffuse axonal injury—initial results. Radiology 2003;227:332–339.
26. Barth M, Nobauer-Huhmann IM, Reichenbach JR, Mlynarik V, Schoggl A, Matula C, Trattnig S. High-resolution three-dimensional contrast-enhanced blood oxygenation of brain tumors at 3 Tesla: first clinical experience and comparison with 1.5 Tesla. Invest Radiol 2003;38:409–414.
27. Abduljalil AM, Schmalbrock P, Novak V, Chakeres DW. Enhanced gray and white matter contrast of phase susceptibility-weighted images in ultra-high-field magnetic resonance imaging. J Magn Reson Imaging 2003;18:284–290.
28. Weiskoff RM, Kiihne S. MRI susceptometry: image-based measurement of absolute susceptibility of MR contrast agents and human blood. Magn Reson Med 1992;24:375.
29. Haacke EM, Brown RW, Thompson MR, Venkatesan R. Magnetic resonance imaging, physical principals and sequence design. New York: Wiley-Liss; 1999. p 741–771.
30. Rauscher A, Barth M, Reichenbach JR, Stollberger R, Moser E. Automated unwrapping of MR phase images applied to BOLD MR-venography at 3 Tesla. J Magn Reson Imaging 2003;18:175–180.